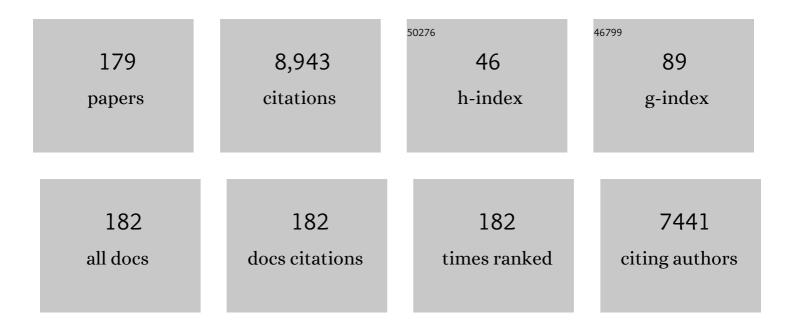
List of Publications by Year in descending order

Source: https://exaly.com/author-pdf/3386931/publications.pdf Version: 2024-02-01



#	Article	IF	CITATIONS
1	Timeâ€lag effects of global vegetation responses to climate change. Global Change Biology, 2015, 21, 3520-3531.	9.5	672
2	Use of General Regression Neural Networks for Generating the GLASS Leaf Area Index Product From Time-Series MODIS Surface Reflectance. IEEE Transactions on Geoscience and Remote Sensing, 2014, 52, 209-223.	6.3	486
3	A long-term Global LAnd Surface Satellite (GLASS) data-set for environmental studies. International Journal of Digital Earth, 2013, 6, 5-33.	3.9	385
4	The altitudinal dependence of recent rapid warming over the Tibetan Plateau. Climatic Change, 2009, 97, 321-327.	3.6	338
5	Validating MODIS land surface reflectance and albedo products: methods and preliminary results. Remote Sensing of Environment, 2002, 83, 149-162.	11.0	315
6	Clear Sky Visibility Has Decreased over Land Globally from 1973 to 2007. Science, 2009, 323, 1468-1470.	12.6	297
7	Long-Time-Series Global Land Surface Satellite Leaf Area Index Product Derived From MODIS and AVHRR Surface Reflectance. IEEE Transactions on Geoscience and Remote Sensing, 2016, 54, 5301-5318.	6.3	297
8	Integration of MODIS LAI and vegetation index products with the CSM–CERES–Maize model for corn yield estimation. International Journal of Remote Sensing, 2011, 32, 1039-1065.	2.9	209
9	The Global Land Surface Satellite (GLASS) Product Suite. Bulletin of the American Meteorological Society, 2021, 102, E323-E337.	3.3	203
10	Cornâ€yield estimation through assimilation of remotely sensed data into the CSMâ€CERESâ€Maize model. International Journal of Remote Sensing, 2008, 29, 3011-3032.	2.9	199
11	An Improved Land Surface Emissivity Parameter for Land Surface Models Using Global Remote Sensing Observations. Journal of Climate, 2006, 19, 2867-2881.	3.2	192
12	Consistency of MODIS surface bidirectional reflectance distribution function and albedo retrievals: 2. Validation. Journal of Geophysical Research, 2003, 108, .	3.3	177
13	An Improved Method for Estimating Global Evapotranspiration Based on Satellite Determination of Surface Net Radiation, Vegetation Index, Temperature, and Soil Moisture. Journal of Hydrometeorology, 2008, 9, 712-727.	1.9	165
14	Estimation of incident photosynthetically active radiation from Moderate Resolution Imaging Spectrometer data. Journal of Geophysical Research, 2006, 111, .	3.3	159
15	Improved estimate of global gross primary production for reproducing its long-term variation, 1982–2017. Earth System Science Data, 2020, 12, 2725-2746.	9.9	156
16	Characterization and intercomparison of global moderate resolution leaf area index (LAI) products: Analysis of climatologies and theoretical uncertainties. Journal of Geophysical Research G: Biogeosciences, 2013, 118, 529-548.	3.0	149
17	Direct-Estimation Algorithm for Mapping Daily Land-Surface Broadband Albedo From MODIS Data. IEEE Transactions on Geoscience and Remote Sensing, 2014, 52, 907-919.	6.3	147
18	Global Land Surface Fractional Vegetation Cover Estimation Using General Regression Neural Networks From MODIS Surface Reflectance. IEEE Transactions on Geoscience and Remote Sensing, 2015, 53, 4787-4796.	6.3	137

#	Article	IF	CITATIONS
19	Consistency of MODIS surface bidirectional reflectance distribution function and albedo retrievals: 1. Algorithm performance. Journal of Geophysical Research, 2003, 108, .	3.3	121
20	Simultaneous estimation of both soil moisture and model parameters using particle filtering method through the assimilation of microwave signal. Journal of Geophysical Research, 2009, 114, .	3.3	119
21	Evidence for decadal variation in global terrestrial evapotranspiration between 1982 and 2002: 1. Model development. Journal of Geophysical Research, 2010, 115, .	3.3	103
22	Evidence for decadal variation in global terrestrial evapotranspiration between 1982 and 2002: 2. Results. Journal of Geophysical Research, 2010, 115, .	3.3	97
23	An optimization algorithm for separating land surface temperature and emissivity from multispectral thermal infrared imagery. IEEE Transactions on Geoscience and Remote Sensing, 2001, 39, 264-274.	6.3	96
24	Mapping daily snow/ice shortwave broadband albedo from Moderate Resolution Imaging Spectroradiometer (MODIS): The improved direct retrieval algorithm and validation with Greenland in situ measurement. Journal of Geophysical Research, 2005, 110, .	3.3	96
25	Progress in bidirectional reflectance modeling and applications for surface particulate media: Snow and soils. International Journal of Remote Sensing, 2000, 18, 307-342.	1.0	91
26	Atmospheric correction of Landsat ETM+ land surface imagery. II. Validation and applications. IEEE Transactions on Geoscience and Remote Sensing, 2002, 40, 2736-2746.	6.3	90
27	Observed contrast changes in snow cover phenology in northern middle and high latitudes from 2001–2014. Scientific Reports, 2015, 5, 16820.	3.3	86
28	Global atmospheric downward longwave radiation over land surface under allâ€sky conditions from 1973 to 2008. Journal of Geophysical Research, 2009, 114, .	3.3	82
29	Global Atmospheric Evaporative Demand over Land from 1973 to 2008. Journal of Climate, 2012, 25, 8353-8361.	3.2	82
30	A Temporally Integrated Inversion Method for Estimating Leaf Area Index From MODIS Data. IEEE Transactions on Geoscience and Remote Sensing, 2009, 47, 2536-2545.	6.3	66
31	Monitoring Drought over the Conterminous United States Using MODIS and NCEP Reanalysis-2 Data. Journal of Applied Meteorology and Climatology, 2010, 49, 1665-1680.	1.5	64
32	Changes of net primary productivity in China during recent 11 years detected using an ecological model driven by MODIS data. Frontiers of Earth Science, 2013, 7, 112-127.	2.1	64
33	An efficient physically based parameterization to derive surface solar irradiance based on satellite atmospheric products. Journal of Geophysical Research D: Atmospheres, 2015, 120, 4975-4988.	3.3	59
34	Estimation of Global Vegetation Productivity from Global LAnd Surface Satellite Data. Remote Sensing, 2018, 10, 327.	4.0	58
35	Assessment of five global satellite products of fraction of absorbed photosynthetically active radiation: Intercomparison and direct validation against ground-based data. Remote Sensing of Environment, 2015, 163, 270-285.	11.0	57
36	A LUT-based approach to estimate surface solar irradiance by combining MODIS and MTSAT data. Journal of Geophysical Research, 2011, 116, n/a-n/a.	3.3	56

#	Article	IF	CITATIONS
37	Improving Predictions of Water and Heat Fluxes by Assimilating MODIS Land Surface Temperature Products into the Common Land Model. Journal of Hydrometeorology, 2011, 12, 227-244.	1.9	56
38	Forest Biomass Mapping of Northeastern China Using GLAS and MODIS Data. IEEE Journal of Selected Topics in Applied Earth Observations and Remote Sensing, 2014, 7, 140-152.	4.9	54
39	Comparison of Four Machine Learning Methods for Generating the GLASS Fractional Vegetation Cover Product from MODIS Data. Remote Sensing, 2016, 8, 682.	4.0	54
40	Estimating the Hemispherical Broadband Longwave Emissivity of Global Vegetated Surfaces Using a Radiative Transfer Model. IEEE Transactions on Geoscience and Remote Sensing, 2016, 54, 905-917.	6.3	54
41	Estimation of clearâ€sky land surface longwave radiation from MODIS data products by merging multiple models. Journal of Geophysical Research, 2012, 117, .	3.3	53
42	Estimation of Daytime Net Radiation from Shortwave Radiation Measurements and Meteorological Observations. Journal of Applied Meteorology and Climatology, 2009, 48, 634-643.	1.5	52
43	Estimation of Incident Photosynthetically Active Radiation from GOES Visible Imagery. Journal of Applied Meteorology and Climatology, 2008, 47, 853-868.	1.5	51
44	Developing a spatially continuous 1 km surface albedo data set over North America from Terra MODIS products. Journal of Geophysical Research, 2007, 112, .	3.3	50
45	Estimating daily mean land surface albedo from MODIS data. Journal of Geophysical Research D: Atmospheres, 2015, 120, 4825-4841.	3.3	50
46	Observational evidence on the effects of clouds and aerosols on net ecosystem exchange and evapotranspiration. Geophysical Research Letters, 2008, 35, .	4.0	49
47	An algorithm for estimating downward shortwave radiation from GMS 5 visible imagery and its evaluation over China. Journal of Geophysical Research, 2010, 115, .	3.3	48
48	Estimation of evapotranspiration over the terrestrial ecosystems in China. Ecohydrology, 2014, 7, 139-149.	2.4	45
49	Numerical experiments on the spatial scaling of land surface albedo and leaf area index. International Journal of Remote Sensing, 2000, 19, 225-242.	1.0	44
50	Assessment of Wetland Ecosystem Health in the Yangtze and Amazon River Basins. ISPRS International Journal of Geo-Information, 2017, 6, 81.	2.9	44
51	Validation of Solar Radiation Surfaces from MODIS and Reanalysis Data over Topographically Complex Terrain. Journal of Applied Meteorology and Climatology, 2009, 48, 2441-2458.	1.5	43
52	Estimation of daily-integrated PAR from sparse satellite observations: comparison of temporal scaling methods. International Journal of Remote Sensing, 2010, 31, 1661-1677.	2.9	43
53	A simple temperature domain twoâ€source model for estimating agricultural field surface energy fluxes from Landsat images. Journal of Geophysical Research D: Atmospheres, 2017, 122, 5211-5236.	3.3	43
54	Evaluation of Moderate Resolution Imaging Spectroradiometer land surface visible and shortwave albedo products at FLUXNET sites. Journal of Geophysical Research, 2010, 115, .	3.3	42

#	Article	IF	CITATIONS
55	Characterization of locations and extents of afforestation from the Grain for Green Project in China. Remote Sensing Letters, 2014, 5, 221-229.	1.4	42
56	Differentiating moss from higher plants is critical in studying the carbon cycle of the boreal biome. Nature Communications, 2014, 5, 4270.	12.8	42
57	Comparison of Radiative Transfer Models for Simulating Snow Surface Thermal Infrared Emissivity. IEEE Journal of Selected Topics in Applied Earth Observations and Remote Sensing, 2010, 3, 323-336.	4.9	41
58	Multiangle remote sensing: Past, present and future. International Journal of Remote Sensing, 2000, 18, 83-102.	1.0	40
59	Temperature changes in Three Gorges Reservoir Area and linkage with Three Gorges Project. Journal of Geophysical Research D: Atmospheres, 2017, 122, 4866-4879.	3.3	40
60	Estimating turbulent fluxes through assimilation of geostationary operational environmental satellites data using ensemble Kalman filter. Journal of Geophysical Research, 2011, 116, .	3.3	39
61	Mapping Daily Evapotranspiration Over a Mediterranean Vineyard Watershed. IEEE Geoscience and Remote Sensing Letters, 2011, 8, 168-172.	3.1	39
62	Responses of Natural Vegetation to Different Stages of Extreme Drought during 2009–2010 in Southwestern China. Remote Sensing, 2015, 7, 14039-14054.	4.0	39
63	Estimating Vegetation Primary Production in the Heihe River Basin of China with Multi-Source and Multi-Scale Data. PLoS ONE, 2016, 11, e0153971.	2.5	39
64	Evaluation of three complementary relationship approaches for evapotranspiration over the Yellow River basin. Hydrological Processes, 2006, 20, 2347-2361.	2.6	38
65	Improving a Penman–Monteith evapotranspiration model by incorporating soil moisture control on soil evaporation in semiarid areas. International Journal of Digital Earth, 2013, 6, 134-156.	3.9	38
66	Global Estimates for High-Spatial-Resolution Clear-Sky Land Surface Upwelling Longwave Radiation From MODIS Data. IEEE Transactions on Geoscience and Remote Sensing, 2016, 54, 4115-4129.	6.3	38
67	Evaluation of satelliteâ€estimated surface longwave radiation using groundâ€based observations. Journal of Geophysical Research, 2010, 115, .	3.3	37
68	Estimating the Fractional Vegetation Cover from GLASS Leaf Area Index Product. Remote Sensing, 2016, 8, 337.	4.0	37
69	Estimating Fractional Vegetation Cover From Landsat-7 ETM+ Reflectance Data Based on a Coupled Radiative Transfer and Crop Growth Model. IEEE Transactions on Geoscience and Remote Sensing, 2017, 55, 5539-5546.	6.3	37
70	GLASS Daytime All-Wave Net Radiation Product: Algorithm Development and Preliminary Validation. Remote Sensing, 2016, 8, 222.	4.0	36
71	An Improved Atmospheric Correction Algorithm for Hyperspectral Remotely Sensed Imagery. IEEE Geoscience and Remote Sensing Letters, 2004, 1, 112-117.	3.1	35
72	Development of the Adjoint Model of a Canopy Radiative Transfer Model for Sensitivity Study and Inversion of Leaf Area Index. IEEE Transactions on Geoscience and Remote Sensing, 2008, 46, 2028-2037.	6.3	35

#	Article	IF	CITATIONS
73	A Framework for Consistent Estimation of Leaf Area Index, Fraction of Absorbed Photosynthetically Active Radiation, and Surface Albedo from MODIS Time-Series Data. IEEE Transactions on Geoscience and Remote Sensing, 2015, 53, 3178-3197.	6.3	35
74	Uncertainty analysis of terrestrial net primary productivity and net biome productivity in China during 1901–2005. Journal of Geophysical Research G: Biogeosciences, 2016, 121, 1372-1393.	3.0	35
75	Estimation of Forest Canopy Height and Aboveground Biomass from Spaceborne LiDAR and Landsat Imageries in Maryland. Remote Sensing, 2018, 10, 344.	4.0	35
76	A Weak-Constraint-Based Data Assimilation Scheme for Estimating Surface Turbulent Fluxes. IEEE Geoscience and Remote Sensing Letters, 2007, 4, 649-653.	3.1	34
77	Estimation of net surface shortwave radiation from MODIS data. International Journal of Remote Sensing, 2012, 33, 804-825.	2.9	34
78	Validation and Spatiotemporal Analysis of CERES Surface Net Radiation Product. Remote Sensing, 2016, 8, 90.	4.0	34
79	Observed radiative cooling over the Tibetan Plateau for the past three decades driven by snow coverâ€induced surface albedo anomaly. Journal of Geophysical Research D: Atmospheres, 2017, 122, 6170-6185.	3.3	34
80	Evaluation of Three Long Time Series for Global Fraction of Absorbed Photosynthetically Active Radiation (FAPAR) Products. IEEE Transactions on Geoscience and Remote Sensing, 2018, 56, 5509-5524.	6.3	33
81	New Global MuSyQ GPP/NPP Remote Sensing Products From 1981 to 2018. IEEE Journal of Selected Topics in Applied Earth Observations and Remote Sensing, 2021, 14, 5596-5612.	4.9	29
82	Reconstruction of Long-Term Temporally Continuous NDVI and Surface Reflectance From AVHRR Data. IEEE Journal of Selected Topics in Applied Earth Observations and Remote Sensing, 2017, 10, 5551-5568.	4.9	28
83	Observational evidence of the cooling effect of agricultural irrigation in Jilin, China. Climatic Change, 2012, 114, 799-811.	3.6	27
84	Spatio-Temporal Analysis and Uncertainty of Fractional Vegetation Cover Change over Northern China during 2001–2012 Based on Multiple Vegetation Data Sets. Remote Sensing, 2018, 10, 549.	4.0	26
85	Evaluation and Comparison of Light Use Efficiency and Gross Primary Productivity Using Three Different Approaches. Remote Sensing, 2020, 12, 1003.	4.0	26
86	Retrieving crop leaf area index by assimilation of MODIS data into a crop growth model. Science China Earth Sciences, 2010, 53, 721-730.	5.2	25
87	An Integrated Method Combining Remote Sensing Data and Local Knowledge for the Large-Scale Estimation of Seismic Loss Risks to Buildings in the Context of Rapid Socioeconomic Growth: A Case Study in Tangshan, China. Remote Sensing, 2015, 7, 2543-2601.	4.0	25
88	Reconstruction of Satellite-Retrieved Land-Surface Reflectance Based on Temporally-Continuous Vegetation Indices. Remote Sensing, 2015, 7, 9844-9864.	4.0	25
89	A Study of Shelterbelt Transpiration and Cropland Evapotranspiration in an Irrigated Area in the Middle Reaches of the Heihe River in Northwestern China. IEEE Geoscience and Remote Sensing Letters, 2015, 12, 369-373.	3.1	25
90	Estimation and validation of land surface broadband albedos and leaf area index from eo-1 ali data. IEEE Transactions on Geoscience and Remote Sensing, 2003, 41, 1260-1267.	6.3	24

#	Article	IF	CITATIONS
91	Designing the Climate Observing System of the Future. Earth's Future, 2018, 6, 80-102.	6.3	24
92	Retrieval of Leaf Area Index (LAI) and Fraction of Absorbed Photosynthetically Active Radiation (FAPAR) from VIIRS Time-Series Data. Remote Sensing, 2016, 8, 351.	4.0	23
93	Distribution, attribution, and radiative forcing of snow cover changes over China from 1982 to 2013. Climatic Change, 2016, 137, 363-377.	3.6	21
94	PMODTRAN: a parallel implementation based on MODTRAN for massive remote sensing data processing. International Journal of Digital Earth, 2016, 9, 819-834.	3.9	21
95	Global simulations of carbon allocation coefficients for deciduous vegetation types. Tellus, Series B: Chemical and Physical Meteorology, 2022, 67, 28016.	1.6	20
96	Planeâ€parallel canopy radiation transfer modeling: Recent advances and future directions. International Journal of Remote Sensing, 2000, 18, 281-305.	1.0	19
97	Evaluation of surface albedo from GEWEX-SRB and ISCCP-FD data against validated MODIS product over the Tibetan Plateau. Journal of Geophysical Research, 2011, 116, n/a-n/a.	3.3	19
98	Satellite detection of increases in global land surface evapotranspiration during 1984–2007. International Journal of Digital Earth, 2012, 5, 299-318.	3.9	19
99	Validity of Five Satellite-Based Latent Heat Flux Algorithms for Semi-arid Ecosystems. Remote Sensing, 2015, 7, 16733-16755.	4.0	19
100	Estimating time-series leaf area index based on recurrent nonlinear autoregressive neural networks with exogenous inputs. International Journal of Remote Sensing, 2012, 33, 5712-5731.	2.9	17
101	Estimating Global Gross Primary Production from Sun-Induced Chlorophyll Fluorescence Data and Auxiliary Information Using Machine Learning Methods. Remote Sensing, 2021, 13, 963.	4.0	17
102	Comparison of Machine Learning Methods to Up-Scale Gross Primary Production. Remote Sensing, 2021, 13, 2448.	4.0	17
103	An Empirical Orthogonal Function-Based Algorithm for Estimating Terrestrial Latent Heat Flux from Eddy Covariance, Meteorological and Satellite Observations. PLoS ONE, 2016, 11, e0160150.	2.5	16
104	Investigation on the Patterns of Global Vegetation Change Using a Satellite-Sensed Vegetation Index. Remote Sensing, 2010, 2, 1530-1548.	4.0	15
105	Estimating Top-of-Atmosphere Daily Reflected Shortwave Radiation Flux Over Land From MODIS Data. IEEE Transactions on Geoscience and Remote Sensing, 2017, 55, 4022-4031.	6.3	15
106	Estimating Diurnal Courses of Gross Primary Production for Maize: A Comparison of Sun-Induced Chlorophyll Fluorescence, Light-Use Efficiency and Process-Based Models. Remote Sensing, 2017, 9, 1267.	4.0	15
107	Continuous tree distribution in China: A comparison of two estimates from Moderate-Resolution Imaging Spectroradiometer and Landsat data. Journal of Geophysical Research, 2006, 111, .	3.3	14
108	Scale transformation of Leaf Area Index product retrieved from multiresolution remotely sensed data: analysis and case studies. International Journal of Remote Sensing, 2009, 30, 5383-5395.	2.9	14

#	Article	IF	CITATIONS
109	Integrating ASTER and GLASS broadband emissivity products using a multi-resolution Kalman filter. International Journal of Digital Earth, 2016, 9, 1098-1116.	3.9	14
110	Simultaneous Estimation of Leaf Area Index, Fraction of Absorbed Photosynthetically Active Radiation, and Surface Albedo From Multiple-Satellite Data. IEEE Transactions on Geoscience and Remote Sensing, 2017, 55, 4334-4354.	6.3	14
111	A New Method for Retrieving Daily Land Surface Albedo From VIIRS Data. IEEE Transactions on Geoscience and Remote Sensing, 2017, 55, 1765-1775.	6.3	14
112	Improvement of dark object method in atmospheric correction of hyperspectral remotely sensed data. Science in China Series D: Earth Sciences, 2008, 51, 349-356.	0.9	13
113	Local Adaptive Calibration of the Satellite-Derived Surface Incident Shortwave Radiation Product Using Smoothing Spline. IEEE Transactions on Geoscience and Remote Sensing, 2016, 54, 1156-1169.	6.3	13
114	Direct Estimation of Land Surface Albedo From Simultaneous MISR Data. IEEE Transactions on Geoscience and Remote Sensing, 2017, 55, 2605-2617.	6.3	13
115	Generation of High Resolution Vegetation Productivity from a Downscaling Method. Remote Sensing, 2018, 10, 1748.	4.0	13
116	Simulating spatially distributed solar-induced chlorophyll fluorescence using a BEPS-SCOPE coupling framework. Agricultural and Forest Meteorology, 2020, 295, 108169.	4.8	13
117	Fast algorithms for estimating aerosol optical depth and correcting Thematic Mapper imagery. Journal of Supercomputing, 1997, 10, 315.	3.6	12
118	Variational retrieval of leaf area index from MODIS time series data: examples from the Heihe river basin, north-west China. International Journal of Remote Sensing, 2012, 33, 730-745.	2.9	11
119	Extended Data-Based Mechanistic Method for Improving Leaf Area Index Time Series Estimation with Satellite Data. Remote Sensing, 2017, 9, 533.	4.0	11
120	Developing an Integrated Remote Sensing Based Biodiversity Index for Predicting Animal Species Richness. Remote Sensing, 2018, 10, 739.	4.0	11
121	Diurnal and Seasonal Variations in Carbon Dioxide Exchange in Ecosystems in the Zhangye Oasis Area, Northwest China. PLoS ONE, 2015, 10, e0120660.	2.5	11
122	Angular corrections to satellite data for estimating earth radiation budget. International Journal of Remote Sensing, 2000, 18, 103-136.	1.0	10
123	A Framework for Estimating the 30Âm Thermalâ€Infrared Broadband Emissivity From Landsat Surface Reflectance Data. Journal of Geophysical Research D: Atmospheres, 2017, 122, 11,405.	3.3	10
124	An assessment of air-quality monitoring station locations based on satellite observations. International Journal of Remote Sensing, 2018, 39, 6463-6478.	2.9	10
125	Spatiotemporal Dynamics of Net Primary Productivity in China's Urban Lands during 1982–2015. Remote Sensing, 2021, 13, 400.	4.0	10
126	Using multiresolution tree to integrate MODIS and MISR-L3 LAI products. , 2010, , .		9

#	Article	IF	CITATIONS
127	A Lookup Table-Based Method for Estimating Sea Surface Hemispherical Broadband Emissivity Values (8–13.5 μm). Remote Sensing, 2017, 9, 245.	4.0	9
128	Application of ensemble kalman filter to geophysical parameters retrieval in remote sensing: A case study of kernel-driven BRDF model inversion. Science in China Series D: Earth Sciences, 2006, 49, 632-640.	0.9	8
129	Investigating the impacts of the North Atlantic Oscillation on global vegetation changes by a remotely sensed vegetation index. International Journal of Remote Sensing, 2012, 33, 7222-7239.	2.9	8
130	Investigation of Atmospheric Effects on Retrieval of Sun-Induced Fluorescence Using Hyperspectral Imagery. Sensors, 2016, 16, 480.	3.8	8
131	Evaluation of Four Reanalysis Surface Albedo Data Sets in Arctic Using a Satellite Product. IEEE Geoscience and Remote Sensing Letters, 2016, , 1-5.	3.1	8
132	Retrieval of aerosol optical depth over bright land surfaces by coupling bidirectional reflectance distribution function model and aerosol retrieval model. Remote Sensing Letters, 2012, 3, 577-584.	1.4	7
133	Simultaneous determination of aerosol optical thickness and surface reflectance using ASTER visible to near-infrared data over land. International Journal of Remote Sensing, 2011, 32, 6961-6974.	2.9	6
134	Fractional vegetation cover estimation based on soil and vegetation lines in a corn-dominated area. Geocarto International, 2017, 32, 531-540.	3.5	6
135	Analyzing the Relationship between Solar-induced Chlorophyll Fluorescence and Gross Primary Production using Remotely Sensed Data and Model Simulation. International Journal of Earth & Environmental Sciences, 2017, 2, .	1.0	6
136	An improved method for estimating global evapotranspiration based on satellite determination of surface net radiation, vegetation index, temperature, and soil moisture. , 2008, , .		5
137	Singular Spectrum Analysis for Filling Gaps and Reducing Uncertainties of MODIS Land Products. , 2008, , .		5
138	Bidirectional Reflectance for Multiple Snow-Covered Land Types From MISR Products. IEEE Geoscience and Remote Sensing Letters, 2012, 9, 994-998.	3.1	5
139	A Bayesian approach to integrate satellite-estimated instantaneous photosynthetically active radiation product for daily value calculation. Journal of Geophysical Research, 2011, 116, .	3.3	4
140	Recent Progress in Quantitative Land Remote Sensing in China. Remote Sensing, 2018, 10, 1490.	4.0	4
141	Retrieval of atmospheric water vapor and land surface temperature from AVHRR thermal imagery. , 0, ,		3
142	Validation of MODIS albedo product by using field measurements and airborne multi-angular remote sensing observations. , 0, , .		3
143	Estimation of crop yield at the regional scale from MODIS observations. , 0, , .		3
144	Use of an ensemble Kalman filter for real-time inversion of leaf area index from MODIS time series data. , 2009, , .		3

#	Article	IF	CITATIONS
145	A disaggregation approach for estimating high spatial resolution broadband emissivity for bare soils from Landsat surface reflectance. International Journal of Digital Earth, 2018, 11, 691-702.	3.9	3
146	A Model-Downscaling Method for Fine-Resolution LAI Estimation. Remote Sensing, 2020, 12, 4147.	4.0	3
147	Estimation and Spatiotemporal Variation Analysis of Net Primary Productivity in the Upper Luanhe River Basin in China From 2001 to 2017 Combining With a Downscaling Method. IEEE Journal of Selected Topics in Applied Earth Observations and Remote Sensing, 2022, 15, 353-363.	4.9	3
148	Retrieval of the Leaf Area Index from Visible Infrared Imaging Radiometer Suite (VIIRS) Surface Reflectance Based on Unsupervised Domain Adaptation. Remote Sensing, 2022, 14, 1826.	4.0	3
149	Inversion of land surface temperature and emissivity simultaneously from multispectral thermal infrared imagery. , 0, , .		2
150	Estimation of Surface Net Radiation from Solar Shortwave Radiation Measurements. , 2008, , .		2
151	The Bidirectional Reflectance Signature of Typical Land Surfaces and Comparison of MISR and MODIS BRDF Products. , 2008, , .		2
152	Prototyping GOES-R albedo algorithm based on modis data. , 2011, , .		2
153	Spatial Representativeness of Gross Primary Productivity from Carbon Flux Sites in the Heihe River Basin, China. Remote Sensing, 2021, 13, 5016.	4.0	2
154	Retrieval of land surface temperature and water vapor content from AVHRR thermal imagery using an artificial neural network. , 0, , .		1
155	Land cover classification methods for multiyear AVHRR data. , 1998, , .		1
156	Comparison of different complementary relationship models for estimating regional evapotranspiration. , 0, , .		1
157	A new composite method for multi-temporal remote sensing data. , 0, , .		1
158	A new method based on remote sensing observations and data assimilation for estimation of evapotranspiration over field crops. New Zealand Journal of Agricultural Research, 2007, 50, 997-1004.	1.6	1
159	Retrieval of Leaf Area Index by Coupling Radiative Transfer Model and a Dynamic Model. , 2008, , .		1
160	Simultaneous estimation of surface photosynthetically active radiation and albedo from GOES. , 2008, , \cdot		1
161	Snow BRDF characteristics from MODIS and MISR data. , 2011, , .		1
162	Retrieval of Horizontal Visibility Using MODIS Data: A Deep Learning Approach. Atmosphere, 2019, 10, 740.	2.3	1

#	Article	IF	CITATIONS
163	Estimation of Global Net Primary Productivity from 1981 to 2018 with Remote Sensing Data. , 2020, , .		1
164	MODIS operational bidirectional reflectance and albedo products. , 0, , .		0
165	Multiple scattering approximations and coherent backscattering theory for soil bidirectional reflectance. , 0, , .		Ο
166	A new algorithm for retrieving land surface temperature and emissivity and applications to airborne hyperspectral SEBASS data. , 1998, , .		0
167	Atmospheric correction of high-resolution satellite imagery for quantitative retrieval of biophysical parameters. , 0, , .		0
168	Land surface geo/biophysical variable estimation from EO-1 data and validation. , 0, , .		0
169	The research of soil moisture difference using the delaying effect of the precipitation on the vegetation. , 0, , .		0
170	Recent algorithm developments in quantitative remote sensing of land surfaces. , 0, , .		0
171	Estimation of daily evapotranspiration in the Yellow River basin by using MODIS data. , 0, , .		0
172	Deriving land surface biophysical parameters from satellite data for soil carbon sequenstration. , 0, , .		0
173	Estimation of regional evapotranspiration in the mu us sandland. , 0, , .		0
174	Crop LAI Retrieval from MODIS Bidirectional Reflectance Observations using the Particle Filter Algorithm and a Crop Growth Model. , 2008, , .		0
175	Research on the spatial distribution of potential crop biomass energy based on remote sensing and GIS: A case study in Henan province, China. , 2009, , .		0
176	Urban expansion analysis of the Huang-Huai-Hai Plain region by DMSP/OLS nighttime light data. , 2009, ,		0
177	Validation of surface radiation data provided by the CERES over the Tibetan Plateau. , 2009, , .		Ο
178	Estimating downward surface shortwave radiation using MTSAT-1R and ground measurements data by Bayesian maximum entropy method. , 2013, , .		0
179	Vegetation Optical Depth Retrieval from AMSR-E/AMSR2 Observations Using L-MEB Inversion. , 2020, , .		0